Interfacial Phenomena and Heat Transfer, 1 (4): 339–356 (2013)

EFFECT OF DROP SHAPE ON HEAT TRANSFER DURING DROPWISE CONDENSATION UNDERNEATH INCLINED SURFACES

Basant Singh Sikarwar, K. Muralidhar, & Sameer Khandekar*

Department of Mechanical Engineering, Indian Institute of Technology Kanpur, Kanpur 208016, India

*Address all correspondence to Sameer Khandekar, E-mail: samkhan@iitk.ac.in

The instantaneous and time-averaged heat transfer coefficient and wall shear stress in dropwise condensation depend on several parameters such as the physical and chemical texture of the substrate, its inclination, and interfacial properties. These factors affect the shape, size, and drop distribution of the condensing drops. On an inclined surface, contact angle varies over the three-phase contact line and the drops get deformed. The commonly used "two-circle model" approximates drop shape as a part of the sphere with a circular footprint. In the present work, this approximation is relaxed and the shape of the drop is obtained by solving the three-dimensional force equilibrium equation. With the shape prescribed, the critical size of drop at instability is determined. Drop-level flow and heat transfer rates associated with fluid motion within have been determined numerically by solving the 3D Navier-Stokes and energy equations in the true drop geometry with applicable boundary conditions. The dropwise condensation model proceeds from the thermodynamically stable liquid droplets, to growth by direct condensation and coalescence, and drop instability, followed by fresh nucleation. Numerical data obtained from the simulation show that wall shear stress and heat transfer coefficient are sensitive to the prescription of the drop shape. The approach proposed in the present study shows a longer time for the drop to become unstable and a larger critical drop size, both factors lowering the estimates of average wall shear stress and heat flux, in comparison to the two-circle approximation.

KEY WORDS: *dropwise condensation, pendant drop, three-dimensional drop shape, Young-Laplace equation, wall shear stress, wall heat flux*

1. INTRODUCTION

Condensation occurs on a solid wall when the surface temperature falls below the local saturation temperature of the adjacent vapor. On specially treated surfaces, liquid droplets will appear at specific nucleation sites. As condensation proceeds, these droplets grow, coalesce with neighboring drops, and may fall off or start to slide down the wall. The process is cyclic and drop instability will prevent the formation of a liquid film. Such a phase-change process, termed dropwise condensation (Carey, 2007), is heterogeneous, in which vapor condenses in the form of discrete liquid drops on or underneath a cold solid substrate. Dropwise condensation can be sustained only on specially textured surfaces (Rose, 1998; Vemuri and Kim, 2006; Rausch et al., 2008; Sikarwar et al., 2011). The subject is of interest because of specific features of this mode of condensation. The heat transfer coefficient during dropwise condensation can be quite high, for example, up to 30 times greater than the filmwise mode, when tested with Langmuir-Blodgett surfaces (Zhao et al., 1996; Koch et al., 1998; Rose, 2002), and 5–20 times better when a promoter layer is used (Koch et al., 1998). Therefore, dropwise condensation has the potential to diminish the size of heat exchange equipment used in thermal and nuclear power plants.

Several researchers have reported that drops form at individual nucleation sites, while the area between the drops remains inactive with respect to condensation (Tanasawa, 1991; Leach et al., 2006; Carey, 2007). The diameter of the smallest drop at nucleation has been estimated from thermodynamic considerations along with the Young-Laplace

2152–5080/13/$35.00

NOMENCLATURE

A	surface area, A_b: base area of a drop, m^2
c_p	specific heat at constant pressure, J/kg K
F	force acting on the drop, N
H	heat transfer coefficient, $q_{\text{wall}}/(T_{\text{sat}} - T_w)$, kW/m^2K
h_{lv}	latent heat of vaporization, J/kg
k	thermal conductivity of condensate, W/m K
N	nucleation site density, cm^{-2}
q	surface heat transfer, W
q_{wall}	surface heat flux, W/m^2
r, r_b	radius of the drop and base radius at criticality, m
r_{cap}	capillary length, $\sqrt{\sigma/g(\rho_l - \rho_v)}$, m
$r_{\max}$	radius of the drop at instability due to fall off, m
r_{crit}	radius of the drop at instability due to slide off, m
T	temperature, K
T_{sat}	saturation temperature, K
T_w	substrate temperature, K
ΔT	degree of subcooling, $(T_{\text{sat}} - T_w)$, K
Δt	time step, s
u, v, w	advancing velocity components in x, y, and z directions, m/s
U	terminal velocity of drop, m/s

Dimensionless Quantities

$C_f, \overline{\overline{C}}_f$	local and average skin friction coefficient, $\tau_w/(1/2)\rho U^2$
Nu, $\overline{\overline{\text{Nu}}}$	local and average Nusselt number, hr_{cap}/k
$(\text{Nu})_{sd}$, $\left(\overline{\text{Nu}}\right)_{sd}$	local and average Nusselt number of a single sliding drop, hr_b/k
Pr	Prandtl number, $\mu C_p/k$
Re	Reynolds number, $\rho U\,(2r_b)/\mu$
$(T - T_w)/\Delta T$	dimensionless temperature

Greek Symbols

α	inclination angle, degrees
μ	dynamic viscosity, Pa s
	the three-phase
ϕ	azimuthal angle measured along contact line (degrees)
ρ	liquid density, kg/m^3
σ	surface tension at liquid–vapor interface, N/m
$\tau_w, \overline{\tau}_w$	local and average wall shear stresses, N/m^2
θ	contact angle, degrees; θ_{adv} for and θ_{rcd} for receding, $\Delta\theta = (\theta_{adv} - \theta_{rcd})$ is hysteresis, and θ_{avg} is the average contact angle

equation (Carey, 2007). Subsequently, the drop grows by direct condensation at a rate determined by the conduction resistance for heat transfer through the drop, the interfacial heat transfer coefficient, and the available temperature difference. Larger drops tend to also grow by coalescence with their neighbors. When a certain size is reached, drops become gravitationally unstable, fall off, or slide along the surface, wiping other drops along their path. Fresh nucleation sites are thus revealed again and the condensation process repeats in a cyclic manner.

The dropwise condensation process depends on the thermophysical properties of the condensing fluid, the physicochemical and thermal properties of the cold substrate, its orientation, surface texture, degree of subcooling, saturation conditions, and the presence of noncondensable gases. It is a hierarchical process, in the sense that it occurs over a wide range of length and timescales. Close process control of dropwise condensation is difficult and one needs to identify systematically the effect of various parameters on the length and timescales of condensation. As the driving temperature difference for the process is small, experimental measurement of the heat transfer coefficient in dropwise condensation is challenging. Leaching of the textured substrate can alter its wettability characteristics and result in its aging. Hence, the heat transfer coefficient of dropwise condensation reported in the literature shows considerable scatter (Rose, 2002). Mathematical modeling is a route available for understanding the details of dropwise condensation.

Glicksman and Hunt (1972), Vemuri and Kim (2006), and Kim and Kim (2012) have developed mathematical models of dropwise condensation based on a single condensate drop combined with a population balance model for

the entire surface. There are, however, some limitations while using this approach. The drop of the condensate is assumed to be hemispherical with a circular base. This approximation fails on inclined and variably textured surfaces and is further limited by the fact that drop instability cannot be correctly predicted (Annapragada et al., 2012). The effect of inclination has been accounted for to an extent by the two-circle approximation (Extrand and Kumagai, 1995; Dimitrakopoulos and Higdon, 1999; El Sherbini and Jacobi, 2006). The importance of the drop shape on local heat transfer and instability has also been discussed by various authors (El Sherbini and Jacobi, 2004; Leipertz, 2010).

The authors of the present study have developed a multiscale dropwise condensation model, starting from the atomic scale, progressing toward the growth of droplets, coalescence, and drop instability, thus closing the entire condensation cycle (Sikarwar et al., 2011; Sikarwar et al., 2012; Sikarwar et al., 2013). Though the model is comprehensive, the drop-level treatment is simplified in the sense that its shape is determined by the two-circle approximation. However, a full calculation, wherein the drop shape and its footprint are determined from first principles, is yet to be considered within the context of the dropwise condensation model.

The objective of the present study is to determine the drop shape in as much detail as possible during the condensation process underneath a substrate. The shape is used to determine the critical size at which the drop will slide or fall off. Surface Evolver, an open source software, is used to simulate the shape of the drop at criticality underneath an inclined surface. Flow and heat transfer within the deformed drop during sliding are recomputed by solving the three-dimensional Navier-Stokes and energy equations on an unstructured grid. This information is built into a hierarchical model of dropwise condensation developed by the authors in their previous work (Sikarwar et al., 2011, 2012). The sensitivity of the model predictions to the drop shape in terms of the instantaneous heat transfer rate and wall shear stress is evaluated against the two-circle approximation.

2. MODEL DEVELOPMENT

The overall mathematical model described previously by the authors (Sikarwar et al., 2012) comprises four steps. These are determination of the three-dimensional drop shapes from a force equilibrium equation, expressions for the critical radius at drop instability, correlations for heat flux and shear stress under a moving drop, and simulation of the overall condensation cycle. Quantities of interest are the condensation patterns, cycle times, area coverage, instantaneous and time-averaged heat fluxes, and wall shear stress. The sensitivity of these data to an accurate estimation of drop shape is of primary interest in the present study.

2.1 Estimation of Shape of Drop at Criticality Underneath an Inclined Substrate

For a drop sitting on a horizontal surface, the shape is determined by the contact angle and volume, apart from material and interfacial properties. On an inclined surface, the contact angle is replaced by the distribution of angles around the three-phase contact line. A variety of approximations have been reported for the contact angle variation (from advancing angle to receding angle), including linear and a cosine functions (El Sherbini and Jacobi, 2006; Dimitrakopoulos and Higdon, 1999; Extrand and Kumagai, 1995; Brown et al., 1980; Milinazzo and Shinbrot, 1988; Korte and Jacobi, 2001), as shown in Fig. 1(a). El Sherbini and Jacobi (2004) conducted experiments to investigate the three-dimensional shape of drop on or underneath an inclined surface. Their results show the contact angle variation along the circumference of a drop is best fitted by a third-degree polynomial in the azimuthal angle. The vertical cross-sectional profile was predicted by the two-circle method sharing a common tangent, while the footprint was approximated by an ellipse. Many researchers (Dusan and Chow, 1983; Cheng et al., 1990) have argued that the leading and trailing angles of a drop at criticality on or underneath an inclined substrate are equivalent to the advancing and receding contact angles, respectively. Their difference, namely, the contact angle hysteresis, is a constant for given liquid-substrate combination. In the present study this hysteresis is prescribed and remains constant throughout the simulation. The variation of contact angle at the three-phase contact line is taken to be cubic in the azimuthal angle.

The shape of a static drop supported on a solid surface is governed by the Young-Laplace equation that balances weight, surface tension, and the internal pressure (Pozrikidis, 2009). In three dimensions, the equation is difficult to solve and alternative approaches are preferred. A variational approach has been proposed to compute the three-dimensional drop shape, wherein the overall energy of the drop (sum of potential and interfacial energy) is successively

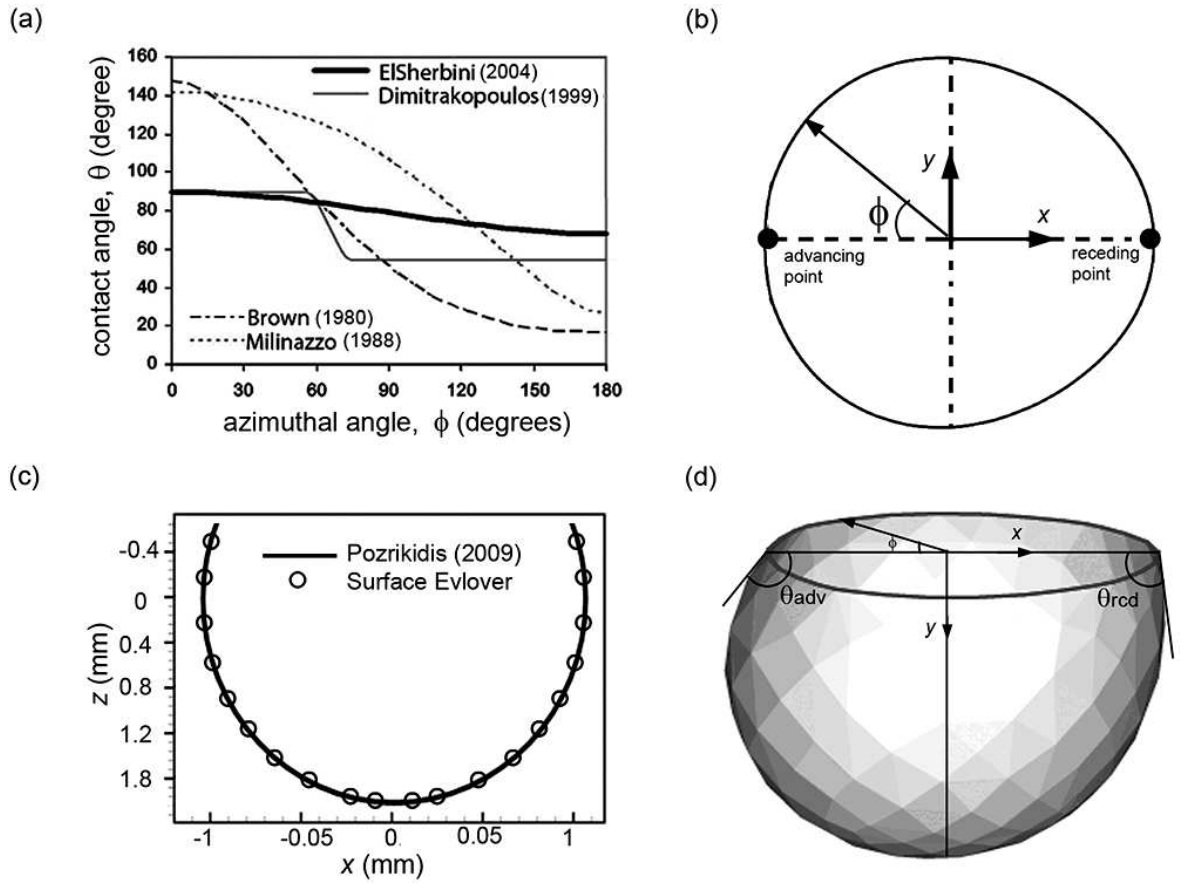

FIG. 1: (**a**) Contact angle as a function of the azimuthal angle as discussed by El Sherbini and Jacobi (2004), Dimitrakopoulos and Higdon (1999), Brown et al. (1980), and Milinazzo and Shinbrot (1988); (**b**) Base contour of three-dimensional drop; (**c**) Validation of the Surface Evolver code for three-dimensional pendant drop shapes. Three-dimensional shape of a 8 μL pendant water drop with a contact angle of 120° is simulated using the Surface Evolver and is compared with the solution of the axisymmetric Young-Laplace equation using the parametric form suggested by Pozrikidis (2009); (**d**) Numerical simulation of three-dimensional pendant drop showing the azimuthal angle which varies from 0° to 360°, advancing angle θ_{adv}, receding angle θ_{rcd}.

minimized. This step has been achieved using Surface-Evolver (Brakke, 1992; Santos and White, 2011) open source software. Complete information on the three-dimensional shape and its footprint can be extracted under equilibrium conditions. The overall numerical methodology is as follows: To initiate the solution, an imaginary cube of liquid of a given volume is taken and its overall energy is minimized to derive the drop shape under equilibrium conditions. In order to provide the surface energy at the solid–liquid interface, the variation of contact angle as a function of the azimuthal angle φ [Fig. 1(b)] needs to be specified. The following contact angle variation proposed by El Sherbini and Jacobi (2004) has been adopted:

$$\theta(\varphi) = 2\frac{(\theta_{adv} - \theta_{rcd})}{\pi^3}\varphi^3 - 3\frac{(\theta_{adv} - \theta_{rcd})}{\pi^2}\varphi^2 + \theta_{adv} \tag{1}$$

Here, θ_{adv} is the advancing angle, θ_{rcd} is the receding angle, and φ is the azimuthal angle [Fig. 1(b)]. The steps for obtaining the shape of three-dimensional nonsymmetric drops using Surface-Evolver are given below:

1. Define an initial cube of liquid with an initial volume equal to V_d.
2. Specify substrate surface inclination, volume constraint, and physical parameters.
3. Specify interfacial energy on the solid–liquid contact plane $z = 0$ using the contact angle variation of Eq. (1), with θ_{adv} and θ_{rcd} as inputs.
4. Specify gravitational potential energy of the liquid as a function of the plate inclination.
5. Use the gradient descent method of Surface-Evolver to approach the new three-dimensional drop shape.
6. After each iteration within Surface-Evolver, correct for the center of the base contour for calculation of the azimuthal angle φ.
7. Repeat steps 3–6 until the drop shape converges.
8. Check for criticality criteria of slide off [Eq. (2)] and fall off [Eq. (3)] as follows:

$$\sigma_{lv} \sum_{i=1}^{N} (r_b \times d\varphi)_i (\cos\theta \cos\varphi)_i + V_d \rho g \sin\alpha \leq 10^{-6} \tag{2}$$

$$\sigma_{lv} \sum_{i=1}^{N} (r_b \times d\varphi)_i (\sin\theta)_i + V_d \rho g \cos\alpha \leq 10^{-6} \tag{3}$$

Equation (2) represents force balance in the direction parallel to the surface, while Eq. (3) is for the component normal to it. If Eqs. (2) and (3) are not satisfied, step (1) is repeated with a new volume $V_d = V_d + \Delta V_d$ until the convergence criteria are met. Here, ΔV_d is an incremental drop volume, specified as 1/50th of the initial volume. The volume obtained using the algorithm referred to here satisfies the force balance equation at criticality of drop slide off or fall off.

Bhutani et al. (2013) have recently shown the utility of Surface-Evolver for contact angle estimations on textured surfaces. In the present work, Surface-Evolver code was first validated for axisymmetric drops against the axisymmetric form of the Young-Laplace equation. Figure 1(c) compares the shapes of an 8 μL axisymmetric pendant water drop, with an equilibrium contact angle of 120°, predicted using Surface-Evolver and the solution of the axisymmetric Young-Laplace equation. The match is seen to be quite good. Figure 1(d) presents the simulated shape of a three-dimensional water drop underneath an inclined surface.

2.2 Modeling of Sliding Drop Underneath an Inclined Substrate

Once the drop becomes unstable, it is set in motion along or away from the surface. Sliding instability is likely to occur first because gravity needs to overcome contact angle hysteresis. For fall off, gravity has to overcome adhesion generated by the average contact angle itself. During sliding, the fluid medium within the drop is set in motion, generating a circulation pattern. These flow details are needed to determine wall heat transfer rates and wall shear stresses over a part of the condensation cycle.

Flow and heat transfer are computed within the moving deformed drop by solving the appropriate equations of motion in three dimensions. The frame of reference for flow and transport calculations is fixed within the liquid drop, the wall moving relative to it at a constant speed. Such calculations are required for each drop moving over the surface within the overall condensation cycle. Such calculations are computationally expensive. As an alternative, drop-level simulations have been carried out and correlations of space-averaged skin friction coefficient C_f and Nusselt number Nu_{sd} are included in the condensation program. These are expressed as a function of Reynolds number and contact angle for various Prandtl number fluids. These correlations serve as an input to the overall condensation model of Sec. 2.3.

The schematic diagram of a three-dimensional deformed drop with an advancing angle θ_{adv} and a receding angle θ_{rcd} is shown in Fig. 2(a). The drop is deformed and the difference in angles between the advancing (leading) and

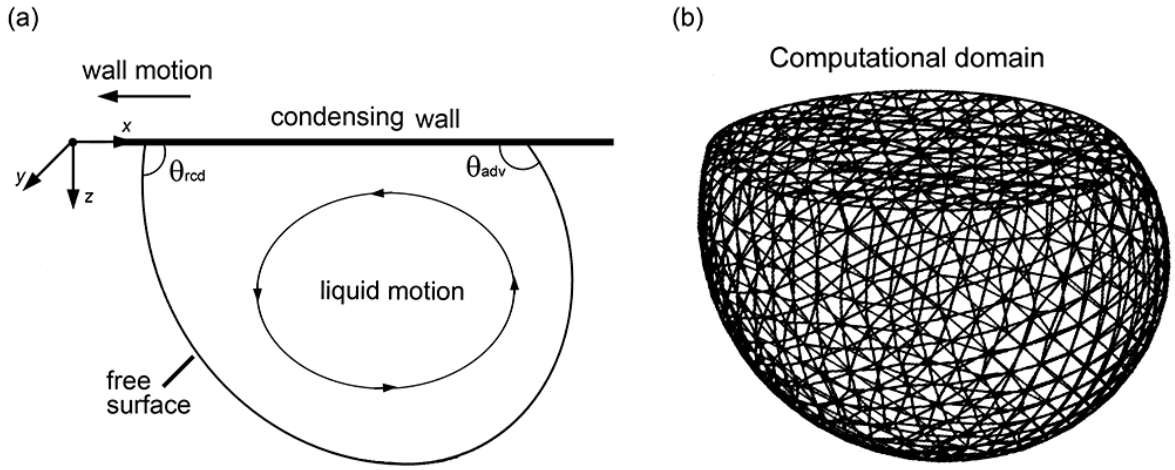

FIG. 2: (**a**) Schematic diagram of fluid motion and heat transfer at the scale of a single drop. (**b**) Computational domain with tetrahedral elements in an unstructured grid.

receding (trailing) sides is the contact angle hysteresis. Simulations have been carried out with advancing angle and hysteresis as parameters varied over 100°–130° and 5°–35°, respectively, for substrate inclinations of 0°, 45°, and 90°, respectively. Dropwise condensation can be sustained only over a hydrophobic surface. Commercially manufactured hydrophobic surfaces have a limited range of contact angles and hysteresis (Annapragada et al., 2012). Specifically, contact angle hysteresis becomes increasingly smaller for substrates with high hydrophobicity. Accordingly, the effect of drop shape on wall shear stress and heat transfer has been explored only for a limited range of parameters. The correlations given later [Eqs. (16)–(19)] are, however, on the basis of a wider range of contact angles (80°–145°) and hysteresis (5°–45°).

The governing equations for flow and heat transfer within a single drop moving over a solid surface are the incompressible, three-dimensional Navier-Stokes and energy equations. The governing equations for flow and heat transfer within an incompressible liquid drop are given in Cartesian tensor notation as follows:

$$\frac{\partial u_i}{\partial x_i} = 0 \tag{4}$$

$$\rho\left(\frac{\partial u_i}{\partial t} + u_j\frac{\partial u_i}{\partial x_j}\right) = -\frac{\partial p}{\partial x_i} + \mu\frac{\partial^2 u_i}{\partial x_j^2} \tag{5}$$

$$\rho c_p\left(\frac{\partial T}{\partial t} + u_j\frac{\partial T}{\partial x_j}\right) = k\frac{\partial^2 T}{\partial x_j^2} \tag{6}$$

The importance of fluid motion generated by the thermocapillary effect and buoyancy can be gauged as follows. For static drops, thermal resistance due to the liquid–vapor interface, constriction resistance, and others are dominant. Fluid motion becomes relevant during the sliding motion of the drop. The relative importance of forced convection with respect to buoyancy and thermocapillary effects can be studied in terms of the ratios $\mathrm{Ma/Re^2}$ and $\mathrm{Gr/Re^2}$, where Ma is Marangoni number and Gr is Grashof number. These ratios were found to be quite small in the present work.

Equations (4)–(6) are written in Cartesian coordinates and solved for the Cartesian velocity components by the finite volume method on an unstructured grid. Boundary conditions are prescribed over the drop surface as follows: At the wall, the no-slip condition holds while the wall has a prescribed temperature. The liquid boundary in contact with vapor is taken to be a stress-free surface. At the free surface, the pressure is constant, the normal component of the velocity is zero, and the shear stress components are also zero. The free surface is also taken to be isothermal at a given distinct saturation temperature. The boundary conditions at the free surface are prescribed in curvilinear coordinates,

n being the unit vector in the direction normal to the boundary, while t_1 and t_2 are orthogonal tangential vectors. They need to be transformed from the local curvilinear to Cartesian coordinates during numerical implementation.

The numerical simulation is based on collocated finite volume discretization of the unsteady three-dimensional Navier-Stokes equations over an unstructured mesh of tetrahedral elements, Fig. 2(b) of nearly equal volumes. Pressure-velocity coupling is treated using a smoothing pressure correction method that results in a SIMPLE-like algorithm (Date, 2005). Convective terms are discretized by a hybrid upwind scheme. The diffusion terms are discretized using a second-order central-difference scheme. Geometry invariant features of the tetrahedral element are used so that the calculation of gradients at cell faces is simplified using nodal quantities of a particular variable. Nodal quantities, in turn, are calculated as a weighted average of the surrounding cell-centered values (Barth and Jespersen, 1989; Frink et al., 1991). The discretized system of algebraic equations is solved in parallel by the stabilized biconjugate gradient method (biCGStab) with a diagonal preconditioner (Sikarwar et al., 2013). Iterations within the code are run until a convergence of 10^{-7} is reached in the residuals. From the velocity and temperature data, wall shear stress and heat transfer rates are determined. The flow and temperature fields are obtained for Reynolds numbers in the range 10–1000 for a range of Prandtl numbers covering liquid metals, water, and organic liquids (Pr $\sim$ 0.005–30). However, the present study is restricted to water as the working fluid, for which Pr is taken as 6.

Local wall shear stress and local wall heat flux are determined as follows:

$$\left.\begin{aligned} (\tau_{xz})_{\text{wall}} &= \mu \left[\frac{\partial u}{\partial z} + \frac{\partial w}{\partial x}\right]_{\text{wall}} \\ (\tau_{yz})_{\text{wall}} &= \mu \left[\frac{\partial v}{\partial z} + \frac{\partial w}{\partial y}\right]_{\text{wall}} \\ \tau_{\text{wall}} &= \sqrt{\tau_{xz}^2 + \tau_{yz}^2} \end{aligned}\right] \tag{7}$$

$$\left.\begin{aligned} q_{\text{wall}} &= -k\left[\frac{\partial T}{\partial n}\right] = -k\left[\frac{\partial T}{\partial z}\right]_{\text{wall}} \\ h &= \frac{q_{\text{wall}}}{\Delta T} \end{aligned}\right\} \tag{8}$$

The length scale chosen for the analysis is the average base radius of the drop at criticality, while dimensionless parameters are evaluated at average temperature between the substrate and the vapor.

It is useful to distinguish between two scales of simulation that are considered—the scale of the drop and the scale of the condensation pattern. Over the vertical extent of the drop, the change in vapor pressure is negligible and hence a constant-pressure boundary condition at the free surface is adequate. Within the drop, the liquid is incompressible and pressure in Eq. (5) is modified pressure that includes gravity. Hence, in the absence of fluid motion, fluid pressure, gravity, and surface tension are in balance, as required by the Young-Laplace equation. On the scale of the condensation pattern, gravity is responsible for drop motion when it overcomes surface tension wall shear at the substrate. Since drop motion on the small scale is modeled in terms of wall velocity, the entire gravity effect is contained in this boundary condition. It is in this respect that the two scales of simulation are coupled, leading to a hierarchical model.

2.3 Modeling of Complete Dropwise Condensation

Multiscale modeling of dropwise condensation over textured surfaces has been discussed earlier by the authors (Sikarwar et al., 2012) and is summarized below. Growth of drops is simulated from drop embryos that grow at specific nucleation sites, while the portion of the surface between the growing drops remains dry. Nucleation sites are randomly distributed on the substrate, while the nucleation site density is fixed as 10^6 cm^{-2} for condensation of water vapor (Poniewski and Thome, 2008). The minimum size of the drop can be found from thermodynamic considerations (Carey, 2007). At the nucleation sites, drops first grow by direct condensation and then coalescence with the neighboring drops. When a certain drop size is reached, the body force component exceeds surface tension and the drop is set in motion. The growth rate of the drop at each nucleation site by direct condensation is limited by the

thermal resistance offered by the drop and the substrate in transferring latent heat release from the vapor to the cold substrate ambient. The rate of condensation at each nucleation site is estimated by using a quasi-one-dimensional approximation for thermal resistances, including the interfacial resistance at the vapor–liquid boundary and conduction resistance through the drop. Drops grow by direct condensation up to a size that is of the order of the distance between adjacent nucleation sites. Beyond this point, coalescence between neighboring drops takes place. Subsequent growth of drops occurs by a combination of direct condensation and coalescence. At the commencement of coalescence, at least two drops will touch each other and are replaced by a drop of equal total volume. The new drop is placed at the resultant center of mass.

Through direct condensation and coalescence, drops are allowed to grow to a critical size where the gravity force exceeds the retention force of surface tension. The drop may then fall off on a horizontal substrate, or slide over an inclined substrate. Hidden sites underneath the original drop (and the sweeping area generated by moving drops, for the case of inclined substrates) become active once the droplets fall or slide off and the entire process is repeated. The equivalent critical base radius of the drop at slide off for an inclined substrate is obtained from Eqs. (2) and (3). These equations show that the critical radius is a function of substrate orientation, contact angle hysteresis, and surface energy.

When the drop achieves terminal velocity, the sum of all external forces acting on it in a direction parallel to inclination of the substrate is zero. These forces are the component of weight parallel to the substrate ($F_{g||}$), surface retention force of the deformed drop due to surface tension (F_r), and wall friction (F_s). Hence

$$F_{g||} + F_r + F_s = 0 \tag{9}$$

Here, $F_{g||}$ is the component of weight parallel to the inclined substrate, F_r is retention force opposing drop motion, and F_s is the viscous force owing to relative velocity between the fluid and the substrate. Viscous forces are available from the detailed computational fluid dynamics (CFD) model and expressed in terms of the skin friction coefficient. Hence, within the dropwise condensation model, terminal velocity of any drop can now be calculated as

$$U = \sqrt{\frac{2(F_{g||} - F_r)}{C_f \rho A_b}} \tag{10}$$

As noted, the sliding drop wipes off other drops that lie in its path, exposing fresh area for renucleation. In addition, the mass and volume of the drop increase during its passage over the surface, owing to incorporation of smaller drops. The sliding velocity of the drop then needs to be recalculated from Eq. (10).

A key assumption in the condensation model is that droplets reach terminal velocity instantly, the driving force (weight component–surface tension) balancing wall shear. Under these conditions, fluid motion within the drop is at its most intense. In this respect, wall shear and heat transfer rates are slightly overpredicted by the model. However, a good match with experiments shows that the approximation is acceptable. Possible reasons for a good match between the model and experiments are twofold: One, the drop-sizebased Reynolds number is mostly small and the acceleration phase is short lived. Second, the duration for which drops move is small (in milliseconds) in comparison to the overall condensation cycle (in minutes).

Heat transfer during dropwise condensation can simply be calculated by knowing the rate of condensation at the free surface of individual drops located over the substrate. The gaps between the growing drops are assumed to be inactive for heat transfer. The mass of condensate accumulated at the ith nucleation site over a time interval Δt is calculated as

$$(\Delta m)_i = \rho \frac{\pi}{3} \left(2 - 3\cos\theta_{avg} + \cos^3\theta_{avg}\right) \left(r^3_{\text{new}} - r^3_{\text{old}}\right)_i \tag{11}$$

With N the number of active nucleation sites at a given time step, the average heat transfer coefficient over an area (A) of the substrate during dropwise condensation is

$$h_{avg} = \frac{h_{lv}}{A\Delta T} \frac{\sum_{i=1}^{N} \sum_{j=1}^{K} (\Delta m)_i^j}{t}; \quad \text{where} \quad t = \left[\sum_{j=1}^{K} (\Delta t)_j\right] \tag{12}$$

Here, t is the time period of condensation and index $K = (t/\Delta t)$ is the number of time steps. The average Nusselt number on the substrate can then be obtained as

$$\overline{\overline{\mathrm{Nu}}} = \frac{h_{avg} r_{\mathrm{cap}}}{k}; \quad \text{where} \quad r_{\mathrm{cap}} = \sqrt{\sigma / g(\rho_l - \rho_v)} \tag{13}$$

In view of a distribution of drop sizes, an obvious length scale is not available for the determination of the Nusselt number. Hence, in Eq. (13), the capillary radius is used as the length scale. It is obtained by equating surface tension with gravity and is of the order of the largest drop at criticality. It represents the average distance across which the temperature differential is applied.

The formulation for determining the surface shear stress acting on the condensing surface due to the continuous sliding of drops is now described. Shear forces are generated by each drop when it begins sliding motion after achieving slide-off criticality. Thereafter, the mass of the droplet may increase during its travel on the substrate. Several drops can be simultaneously in motion over the surface and their sizes change with time. For the surface as a whole, the average shear stress is obtained by spatiotemporal averaging the effect due to an ensemble of moving droplets. The average shear stress on the substrate is defined as

$$\bar{\tau}_s = \frac{\bar{F}_s}{A} = \frac{1}{A} \left[\frac{\sum_{j=1}^{K} \sum_{i=1}^{N} [F_s]_i^j}{t} \right] \tag{14}$$

The average skin friction coefficient on the substrate can then be estimated as

$$\overline{\overline{C}}_f = (\bar{\tau}_s) \,/\, \left(\frac{1}{2} \rho U_{\mathrm{rep}}^2 \right), \quad \text{where} \quad U_{\mathrm{rep}} = \sqrt{g \cdot r_{\mathrm{cap}}} \tag{15}$$

Although no droplet can commence motion unless its radius exceeds the critical value, the ensuing terminal velocity of moving drops will vary depending on the path traversed and the amount of additional mass gathered along the way. Hence, a velocity scale is not readily available. A representative drop velocity U_{rep} is generically obtained by scaling gravitational acceleration, namely, potential energy against the kinetic energy of the drop, yielding the expression given in Eq. (15). All the physicochemical characteristics of the liquid–solid combination are embedded in the critical radius, and in turn, the Reynolds number (Sec. 3.2).

2.4 Validation

Validation of the condensation model against experiments in terms of condensation patterns and cycle times is discussed by the authors elsewhere (Sikarwar et al., 2011). The model has also been validated for surface-averaged heat transfer rates against experiments with water vapor available in the literature (Rose, 2002). Validation of the CFD code that has been used to generate drop-level correlations has been reported by Sikarwar et al. (2013). Validation of the 3D Young-Laplace equation solver is discussed by Bhutani et al. (2013). Drop shapes and their footprints attained during dropwise condensation have not been reported in the literature and hence, have not been compared.

3. RESULTS AND DISCUSSION

The goal of the present work is to examine the sensitivity of the dropwise condensation model to the details of the drop shape. In the simulations discussed, the condensate is water.

The shape obtained from Surface-Evolver is exact since the force equilibrium equation is solved in its entirety. The two-circle methodology provides an approximation to the drop shape on inclined surfaces. Accordingly, results below are reported in three parts:

1. Shape of a drop determined by Surface-Evolver (present) compared with the two-circle approximation (previous);

2. Flow and temperature distribution inside a single sliding drop; and

3. Comparison of dropwise condensation patterns when individual drops are modeled by the two approaches, respectively.

3.1 Drop Shape at Criticality

Figure 3 shows the shape of the drop obtained from Surface-Evolver as compared to the two-circle approximation. In both methods, the advancing angle is 120° while the contact angle hysteresis is taken as 35°. The direction of gravity is to the right, as shown in Fig. 3. The volumes of drops in both methods [Figs. 3(a) and 3(b)] are equal (12.5 μL). The predicted shapes are quite distinct, while the footprint using the force balance equations is noncircular on vertical substrates. In addition, Surface-Evolver shows that the drop deforms on the two orthogonal planes and its cross section on planes parallel to the surface is also noncircular.

Figure 4 shows the footprint of drops of various volumes, respectively, having a contact angle of 110° and hysteresis 20° on a vertical surface. The footprint is seen to become increasingly noncircular with the increase of droplet volume.

Figure 5 compares volumes of the drop at criticality for various substrate inclinations. The critical volume determined using Surface-Evolver (present) is larger than the one calculated by the two-circle approximation (previous). This result arises from the fact that the drop shape predicted in the present approach has greater deformation. In the two-circle approximation, the drop essentially deforms along with the plate inclination, remaining nearly unchanged in the orthogonal plane. Hence, the force of adhesion due to surface tension, related to drop curvature, is higher in the present approach and the drop can grow to a larger size before becoming gravitationally unstable.

3.2 Flow and Heat Transfer in a Drop

Velocity and temperature distributions in a single deformed drop sliding on an inclined surface are discussed in the present section. Drop shapes determined by the two-circle methodology and Surface-Evolver are compared. Figure 6(a) shows contours of the x-component velocity within a liquid drop at Reynolds numbers of 100 and 500,

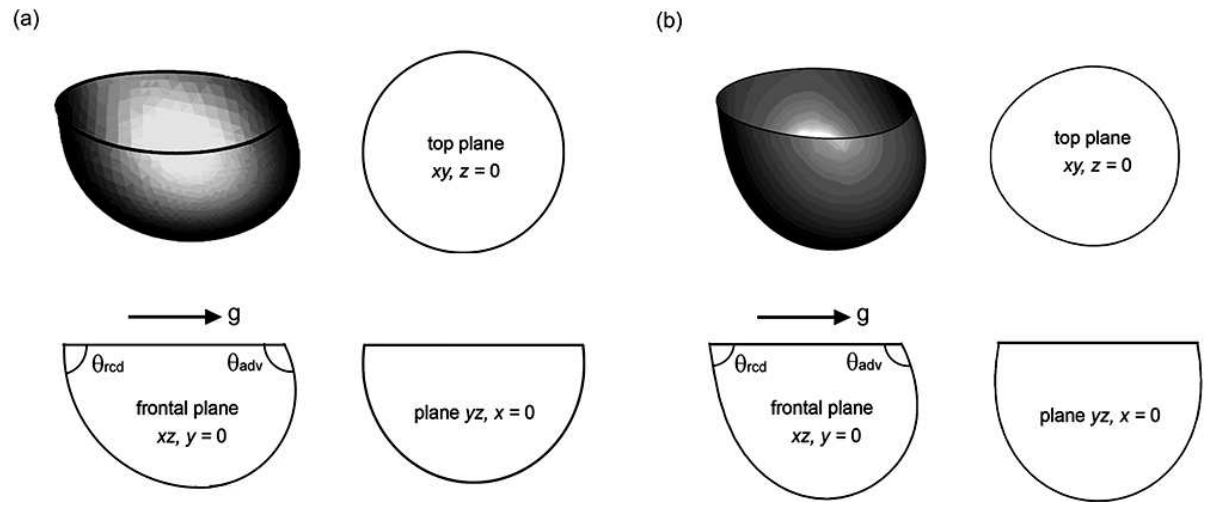

FIG. 3: Isometric view of the shape of a water drop and its two dimensional projections over various planes obtained by (**a**) the two-circle approximation (previous) and (**b**) Surface Evolver (present). Advancing angle 120°, contact angle hysteresis 35°, plate inclination 90°. The direction of gravity is to the right. Volumes of the drop in (**a**) and (**b**) are equal.

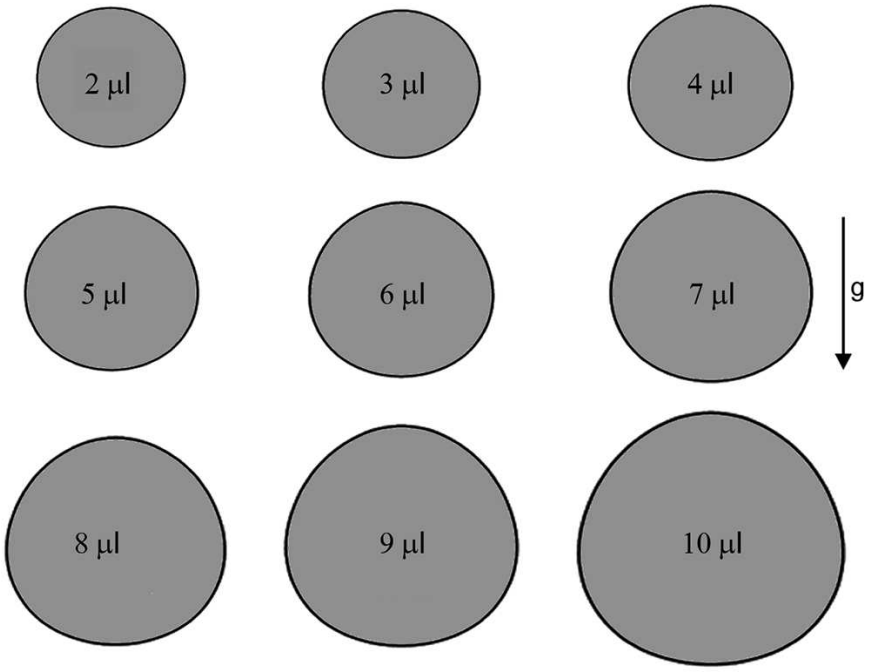

FIG. 4: Effect of volume on the footprint of a drop on a vertical surface; advancing angle 110° and contact angle hysteresis 20°.

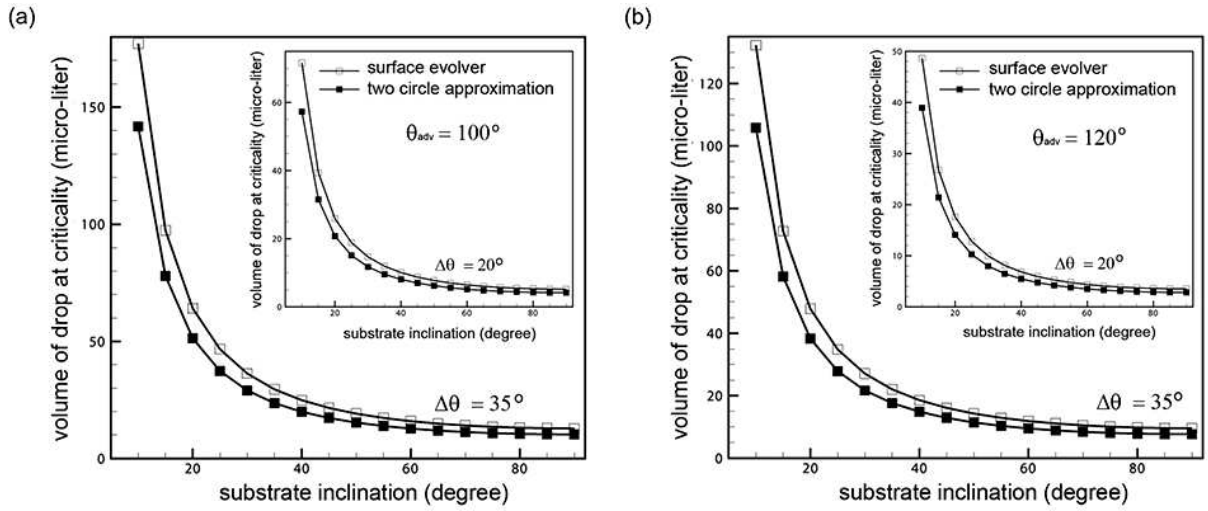

FIG. 5: Variation of volume of water drop at criticality with respect to substrate inclination. (**a**) Advancing angle 100°, contact angle hysteresis 35°, while for inset, contact angle hysteresis is 20°. (**b**) Advancing angle 120° and contact angle hysteresis 35°, while for the inset, contact angle hysteresis is 20°.

advancing angle 110°, and contact angle hysteresis 20°. For the plane selected, the surface motion is to the right, in the plane of the paper. The velocity magnitude near the free surface is close to the wall speed but in the opposite direction. Temperature contours within the water drop over the central plane are shown in Fig. 6(b). Temperature

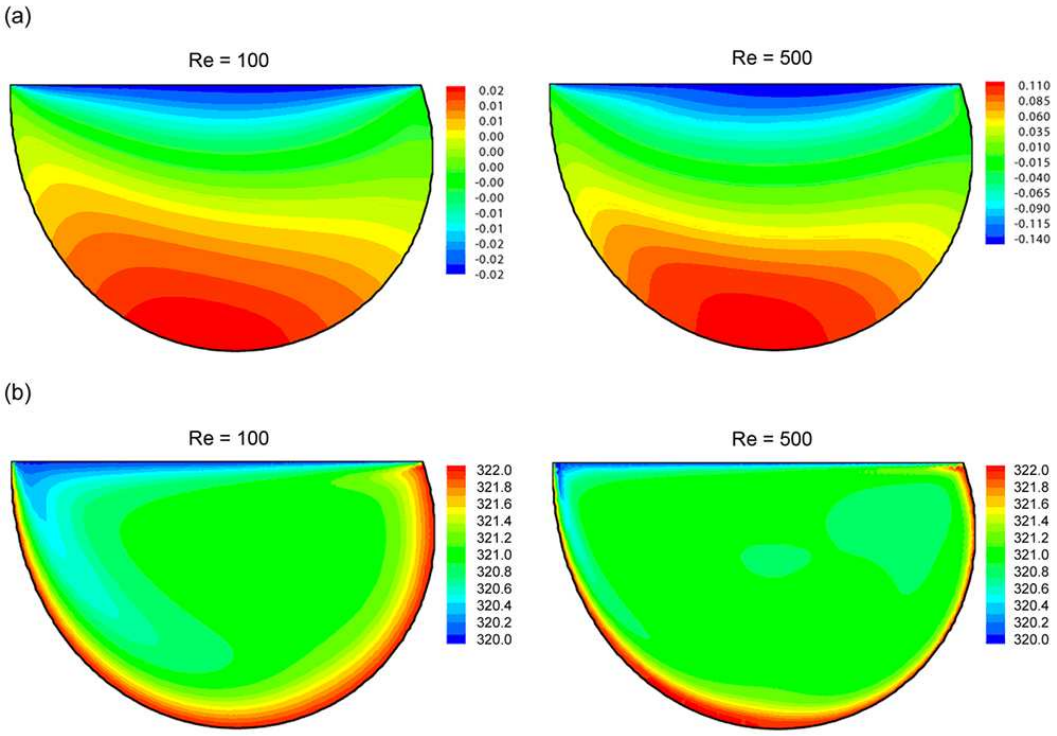

FIG. 6: (**a**) x-component velocity distribution over the frontal $y = 0$ plane on a color scale inside a pendant drop of advancing angle 110°, hysteresis 20°, plate inclination 90°, degree of subcooling 2 K, Re = 100 and 500. (**b**) Temperature field inside the deformed drop at Pr = 6 for Reynolds numbers of 100 and 500.

gradients at the free surface and the wall are higher compared to the center, and clear thermal boundary layers are formed owing to the moderate Prandtl number of water. An equivalent set of data for a drop shape determined by the two-circle approximation has been reported by the authors elsewhere (Sikarwar et al., 2013). The flow distributions in the two approaches, though similar, show minor differences which eventually change the shear stress profile, as will be seen next.

Distributions of wall shear stress and wall heat transfer are shown in Figs. 7(a) and 7(b), respectively. These quantities become quite large near the three-phase contact line of the drop. This result has important consequences in surface wear/leaching characteristics. Specifically, it can be concluded that substrate damage would be initiated along the three-phase contact line. Analogous to the wall shear stress, large heat transfer rates are realized in close vicinity of the three-phase contact line [Fig. 7(b)].

Similar flow and temperature patterns have been estimated for a variety of deformed drops and Reynolds numbers. On the basis of the data obtained, a correlation of average skin friction coefficient at the scale of the drop has been developed in terms of average contact angle and Reynolds number. Here, Reynolds number is based on the critical base diameter of the drop footprint. The correlation is of the form

$$\overline{C_f} = 64.2\ \mathrm{Re}^{-0.97}\theta_{avg}^{-1.58} \tag{16}$$

In a previous approach (two-circle approximation), the average skin friction coefficient was determined as (Sikarwar et al., 2013)

$$\overline{C_f} = 58\ \mathrm{Re}^{-0.97}\theta_{avg}^{-1.57} \tag{17}$$

Both correlations show a near reciprocal dependence of skin friction coefficient on Reynolds number. This trend is common to fully developed flow in internal geometries, as opposed to boundary layers. Equations (16) and (17) also

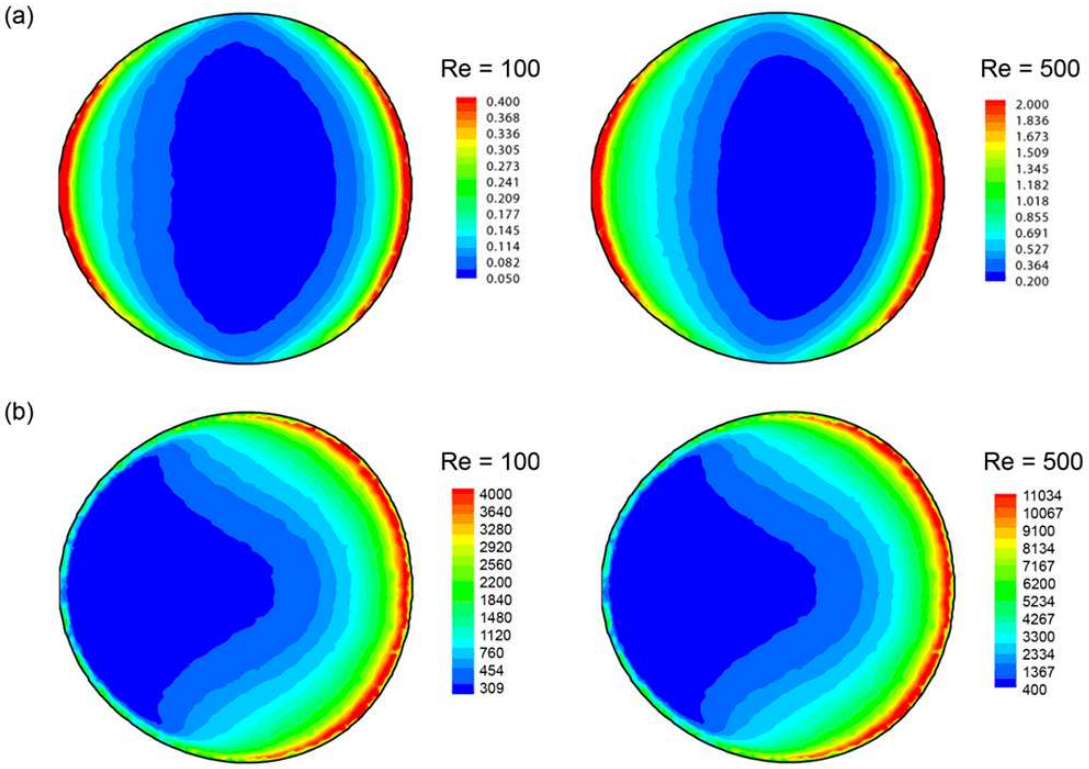

FIG. 7: (**a**) Wall shear stress and (**b**) wall heat flux distribution at various Reynolds numbers; Pr = 6. Other properties are as in Fig. 6.

show that skin friction decreases with increasing contact angle, namely, the hydrophobicity of the surface. Thus highly hydrophobic surfaces would be less prone to wear.

Equations (16) and (17) show that the previous approach estimates the average skin friction coefficient to be smaller in comparison to the true shape obtained by Surface-Evolver. This result can be traced to the fact that drop deformation on an inclined surface is truly three dimensional, as revealed by Surface-Evolver calculation. Hence the distortion of fluid movement within the drop is greater and is revealed as an increased wall shear stress.

On the basis of data obtained for wall heat transfer, the following correlations of the average Nusselt number at the drop scale have been developed in terms of Prandtl and Reynolds numbers. The length scale in Reynolds number is the base diameter of the drop at criticality. For Nusselt number, it is the capillary radius. The range of Prandtl numbers studied is $3.5 < \mathrm{Pr} < 7$. The old and the new correlations are obtained as follows:

$$\text{Present:} \quad \left(\overline{\mathrm{Nu}}\right)_{sd} = 12.4\mathrm{Re}^{0.196}\mathrm{Pr}^{0.1}\theta_{avg}^{-0.77} \tag{18}$$

$$\text{Previous:} \quad \left(\overline{\mathrm{Nu}}\right)_{sd} = 9.48\mathrm{Re}^{0.196}\mathrm{Pr}^{0.1}\theta_{avg}^{-0.77} \tag{19}$$

The dependence of the average heat transfer coefficient on Reynolds number is quite mild. The dependence of heat transfer coefficient on the drop shape is seen to be strong through the contact angle. Nusselt number prediction in the present approach with Surface-Evolver is greater than the previous. Here again, the reason for this difference can be traced to the truly three-dimensional drop shape that distorts the flow field and augments wall shear stress and thus, the heat transfer. The increase in the extent of three-dimensionality contributes to higher Nusselt numbers as well.

Equations (16)–(19) have a regression coefficient of better than 99.1%.

3.3 Condensation Patterns

The spatiotemporal drop distributions, from initial nucleation to drop instability, are shown in Figs. 8(a) and 8(b) for condensation of water vapor over a vertical surface. The drop shape is characterized by an advancing angle (θ_{adv}) = 110° and contact angle hysteresis ($\Delta\theta$) = 20°. The saturation temperature is 315 K, and the degree of subcooling between the vapor and the substrate is 2 K. As discussed in Sec. 3.2, Figs. 8(a) and 8(b) show that the average footprint of the drop over the substrate at a given time instant is greater in the present approach, when compared to the two-circle approximation.

Condensation patterns are time dependent and best discussed in terms of statistical properties. The effect of drop shape on instantaneous area coverage, available nucleation sites, wall heat transfer, and wall shear stress are summarized in Figs. 9 and 10. Figure 9(a) shows that the area of coverage obtained by the modified approach is higher than the two-circle approximation. Figure 9(a) also shows that the area of coverage builds up when drops grow by condensation and coalescence but decreases sharply as drops slide away on the substrate. These trends are also visible in Fig. 8. Since the present approach results in larger drops to be formed, the first fall off is delayed [see inset,

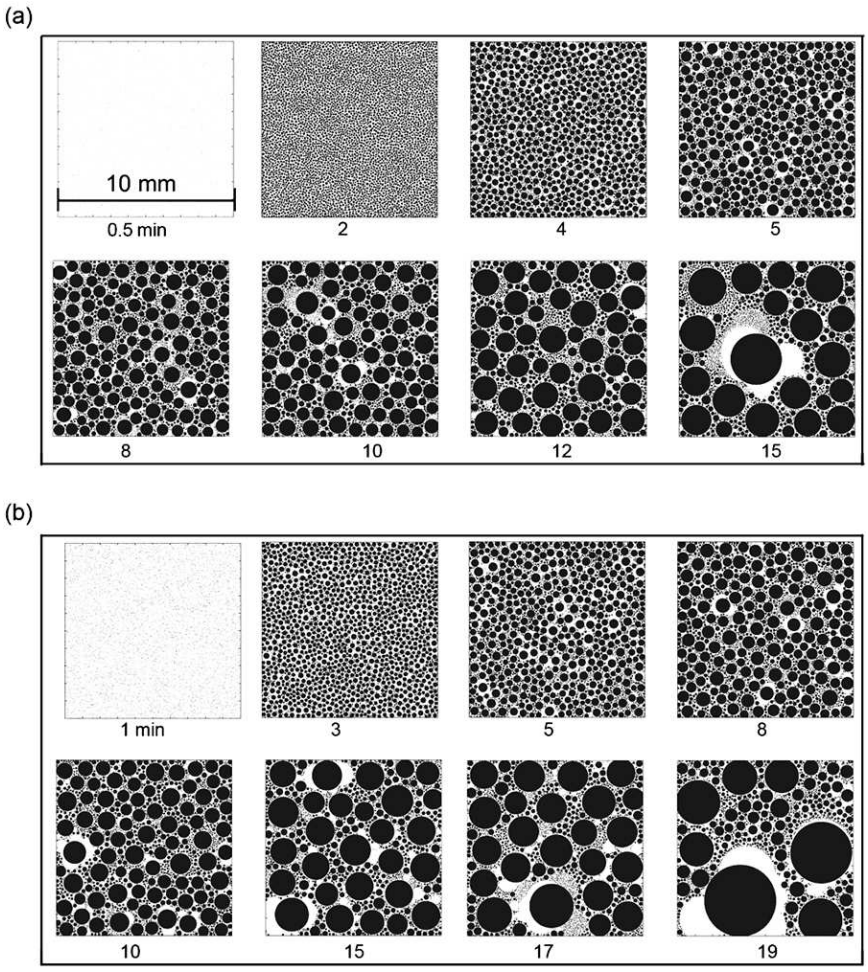

FIG. 8: Drop distributions from initial nucleation to first drop slide off on a surface vertical surface for condensing fluid water. Drop shape determined by (**a**) two-circle approximation (previous) and (**b**) Surface Evolver (present). Advancing angle 110°, hysteresis 20°, and degree of subcooling 2 K.

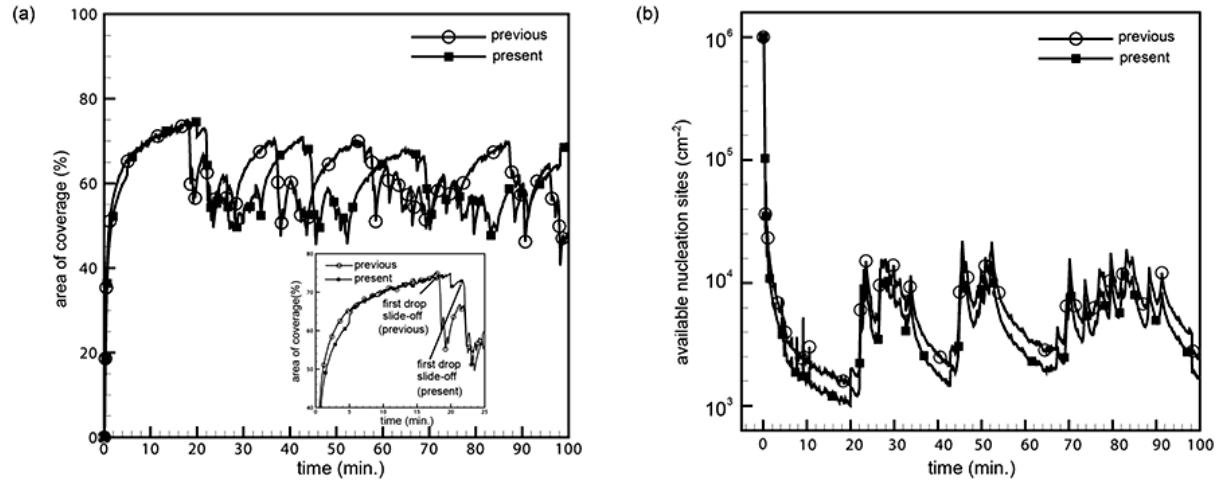

FIG. 9: (**a**) Variation of area of coverage with respect to time by the present approach compared with the two-circle approximation (previous approach) (Sikarwar et al., 2011). Inset, large view from commencement of dropwise condensation to the first slide of a drop; (**b**) Cyclic variation of available nucleation sites with respect to time. Advancing angle 110°, hysteresis 20°, and degree of subcooling 2 K.

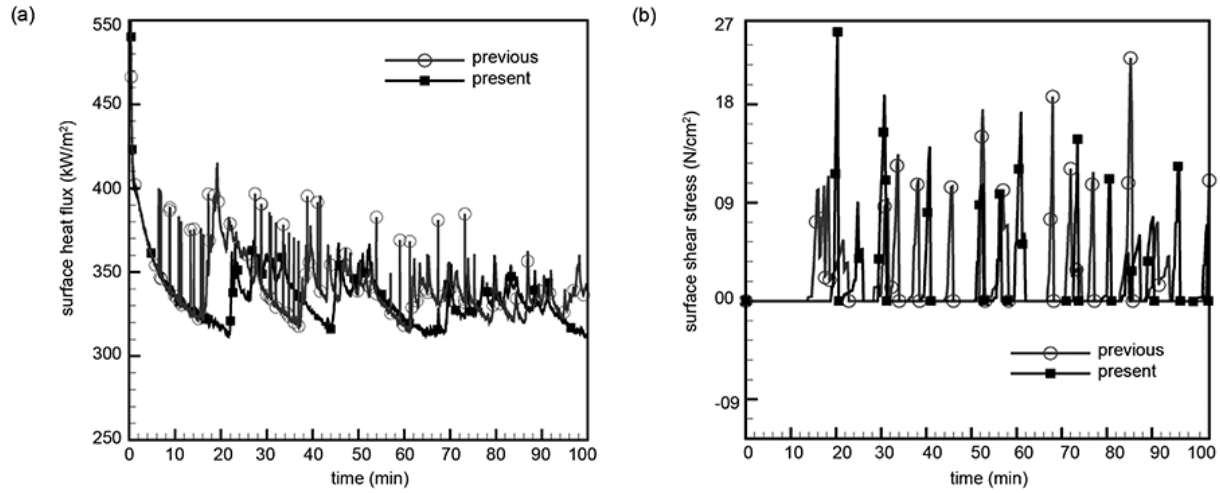

FIG. 10: (**a**) Cyclic variation of instantaneous wall heat transfer rate during condensation of water vapor, and (**b**) instantaneous wall shear stress distribution. Advancing angle 110°, hysteresis 20°, and degree of subcooling 2 K.

Fig. 9(a)]. Figure 9(b) shows the variation of available nucleation sites with respect to time. It is determined from the open area of the substrate where condensation has not taken place. The area coverage and available nucleation sites change rapidly in the beginning, reaching a cyclic state later, with a well-defined average.

The temporal variation of heat transfer through the entire condensing substrate is presented in Fig. 10(a). At an early stage of condensation, drops are small and offer small conduction resistance. Hence the growth rates are high, and a large heat flux passes through the substrate. At later times, a cycle of drop formation and departure is obtained, leading to a dynamic steady state in heat transfer with a well-defined time average. Figure 10(a) shows that the instantaneous heat transfer obtained with the present approach is less than the two-circle approximation because the corresponding drop volume at criticality is greater.

Temporal variation of wall shear stresses during drop motion over the condensing substrate is shown in Fig. 10(b). Unlike heat transfer, shear stresses are nonzero only during drop motion. Thus, in the new approach, shear stresses are affected by a higher coefficient of skin friction [Eq. (16)] but a smaller time for motion since drops are stationary for a longer period. Hence, with respect to the prediction of the drop shape, the trend here is inconclusive. The shear stresses determined using the present approach for the drop shape show marginally lower values at certain time instants within the condensation cycle.

Average Nusselt number and average skin friction coefficient for the entire surface are shown in Fig. 11. The surface orientation is vertical. Figure 11(a) shows the variation of average Nusselt number with respect to degree of subcooling. The condensation parameters are selected as in Fig. 8, except that the degree of subcooling is a variable. The variation of average skin friction coefficient with respect to degree of subcooling is shown in Fig. 11(b). The effect of increasing subcooling is to increase the rate of condensation, increase the growth rates of drops, reduce the cycle time, and increase the number of drops sliding at any given instant. Hence, Nusselt number and skin friction coefficient monotonically increase with subcooling. The Nusselt number and average skin friction coefficient with the present approach are less than the two-circle approximation because the corresponding drop volume at criticality is greater. Similar results were obtained for condensation under a surface at 45° inclination.

Table 1 summarizes the condensation parameters on a horizontal, 45° inclination, and a vertical surface. For a horizontal surface, pendant drops are formed that experience fall-off instability and a critical radius of $r_{\max}$. For the other two configurations, the critical drop size is given by r_{crit}. The previous and the present approaches in drop-shape calculations are compared. The present approach is seen to generate larger drops and a larger area of coverage. The time for fall off and slide off with the present approach is delayed. The present approach yields smaller average Nusselt numbers owing to enhanced conduction resistance of the larger drop. The surface and cycle-averaged skin friction coefficient is smaller in the present approach because of a longer time period for which drops grow but are stationary.

4. CONCLUSIONS

An unsteady hierarchical mathematical model of vapor condensation in the form of drops underneath inclined surfaces is discussed. A numerical model based on Surface-Evolver, an open domain software, is used to solve the force equilibrium equation and obtain three-dimensional shapes of static drops at criticality. With the correct shape determined,

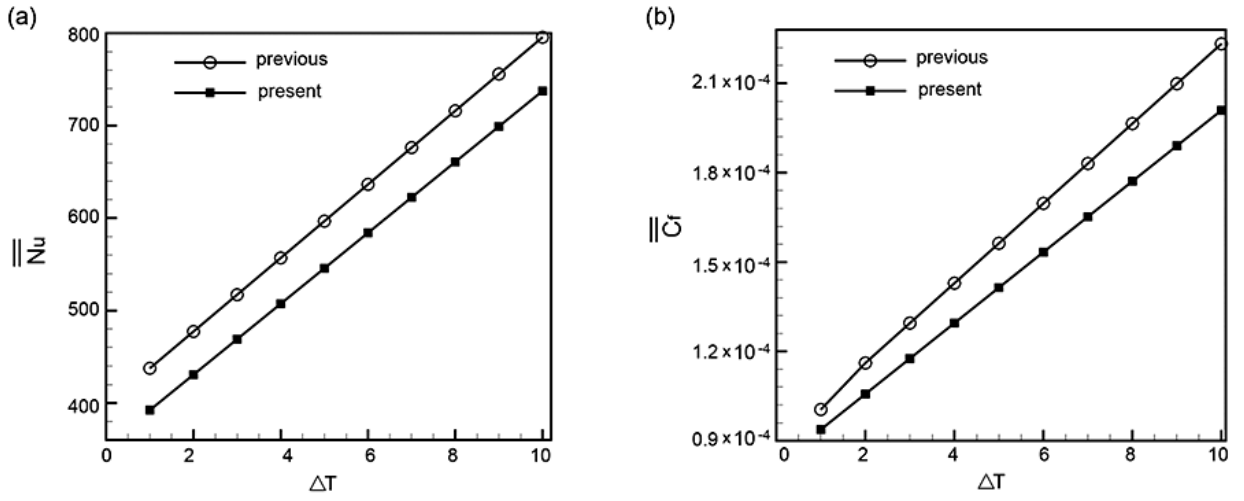

FIG. 11: (**a**) Variation of average surface Nusselt number with respect to degree of subcooling. (**b**) Variation of average surface skin friction coefficient with respect to degree of subcooling for condensation of water vapor on the vertical substrate. Advancing angle 110°, hysteresis 20°.

TABLE 1: Comparison of condensation parameters for water vapor with the old and the new approaches of determining the drop shape. The last two columns are time- and area-averaged transport coefficients. Contact angle data is given in Fig. 8, while subcooling is 2 K.

Approach	Substrate orientation	$r_{\max}$; r_{crit} (mm)	Area of coverage (%) (min)	Time for first fall/slide off	Time elapsed between successive sliding events (min)	$\overline{\overline{C_f}}$	$\overline{\overline{\text{Nu}}}$
Two-circle approximation	0°	4.25	78	57	5.9	0	220
	45°	2.12	72	42	1.7	0.122×10^{-4}	290
	90°	1.49	64	15	0.77	0.987×10^{-4}	430
Present (Surface Evolver)	0°	4.32	82	59.2	6.35	0	187
	45°	2.60	76	43.5	1.98	0.961×10^{-5}	247
	90°	1.54	67	21	0.9	0.902×10^{-4}	380

drop motion is independently simulated by a 3D Navier-Stokes and energy equations solver. The wall shear stress and heat flux information is included in the condensation model in the form of correlations. Quantities of interest such as condensation patterns, wall shear stress, and wall heat transfer have been predicted. These are compared with predictions of an approximate route of finding the drop shape, based on the two-circle approximation.

The new approach shows drop deformation in the two orthogonal directions and a noncircular footprint. Consequently, it predicts larger drops at criticality. The flow field at the scale of the moving drop is intensified due to its deformation in three dimensions, leading to higher Nusselt number and wall shear stress. For the substrate as a whole, the time taken to reach instability is greater for the drop, while the conduction resistance offered is greater as well. Hence the cycle-averaged Nusselt number with the present approach is smaller than the two-circle approximation. Shear stress is nonzero only during drop motion. Since this phase of the cycle is reduced in time, the skin friction coefficient with the new approach is smaller than the old. Overall, drop size and shape are seen to influence the macroscopic parameters in dropwise condensation.

REFERENCES

Annapragada, S. R., Murthy, J. Y., and Garimella, S. V., Droplet retention on an incline, *Int. J. Heat Mass Transfer,* vol. **55**, pp. 1457–1465, 2012.

Bansal, G. D., Khandekar, S., and Muralidhar, K., Measurement of heat transfer during dropwise condensation of water on polyethylene, *Nanoscale Microscale Thermophys. Eng.*, vol. **13**, pp. 184–201, 2009.

Barth, T. J. and Jespersen, D. C., The design and application of upwind schemes on unstructured meshes, *AIAA*, vol. **89**, p. 0366, 1989.

Bhutani, G., Muralidhar, K., and Khandekar, S., Determination of apparent contact angle and shape of a static pendant drop on a physically textured inclined surface, *Interfacial Phenom. Heat Transfer*, vol. **1**, no. 1, pp. 29–49, 2013.

Brakke, K., The surface evolver, *Exp. Math.*, vol. **1**, no. 2, pp. 141–165, http://www.susqu.edu/brakke/evolver/evolver.html, 1992.

Brown, R. A., Orr, Jr., F. M., and Scriven, L. E., Static drop on an inclined plate: Analysis by the finite element method, *J. Colloid Interface Sci.*, vol. **73**, no. 1, pp. 76–87, 1980.

Carey, V. P., *Liquid-Vapor Phase-Change Phenomena*, 2nd ed., Hemisphere Publishing Corp., New York, pp. 342–351, 2007.

Cheng, P., Li, D., Boruvka, L., Rotenberg, Y., and Neumann, A. W., Automation of axisymmetric drop shape analysis for measurements of interfacial tensions and contact angles, *Colloid Surf.*, vol. **43**, pp. 151–167, 1990.

Date, A. W., Solution of transport equations on unstructured meshes with cell centered collocated variables, Part I. Discretization, *Int. J. Heat Mass Transfer*, vol. **48**, pp. 1117–1127, 2005.

Dimitrakopoulos, P. and Higdon, J. J. L., On the gravitational displacement of three-dimensional fluid droplets from inclined solid surfaces, *J. Fluid Mech.*, vol. **395**, pp. 181–209, 1999.

Dusan, E. B. and Chow, R. T. P, On the ability of drops or bubbles to stick to non-horizontal surfaces of solids, *J. Fluid Mech.*, vol. **137**, pp. 1–29, 1983.

El Sherbini, A. I. and Jacobi, A. M., Liquid drops on vertical and inclined surfaces: I. An experimental study of drop geometry, *J. Colloid Interface Sci.*, vol. **273**, no. 2, pp. 556–565, 2004.

El Sherbini, A. I. and Jacobi, A. M., Retention forces and contact angles for critical liquid drops on non-horizontal surfaces, *J. Colloid Interface Sci.*, vol. **299**, pp. 841–849, 2006.

Extrand, C. W. and Kumagai, Y., Liquid drops on an inclined plane: The relation between contact angles, drop shape and retentive force, *J. Colloid Interface Sci.*, vol. **170**, no. 2, pp. 515–521, 1995.

Fox, H. W. and Zisman, W. A., The spreading of liquids on low energy surfaces, I. Polytetrafluoroethylene, *J. Colloid Sci.*, vol. **5**, no. 6, pp. 514–531, 1950.

Frink, N. T., Paresh, P., and Shahyar, P., A fast upwind solver for the Euler equations on three dimensional unstructured meshes, *AIAA*, vol. **91**, p. 0102, 1991.

Glicksman, R. L. and Hunt, W. A., Numerical simulation of dropwise condensation, *Int. J. Heat Mass Transfer*, vol. **15**, pp. 2251–2269, 1972.

Kim, S. and Kim, K. J., Dropwise condensation suitable for superhydrophobic surfaces, *ASME J. Heat Transfer*, vol. **133**, no. 8, pp. 0815021–0815028, 2011.

Koch, G., Kraft, K., and Leipertz, A., Parameter study on the performance of dropwise condensation, *Rev. Gen. Therm.*, vol. **37**, pp. 539–548, 1998.

Korte, C. M. and Jacobi, A. M., Condensation retention effects on the performance of plain-fin and tube heat exchanger: Retention data and modeling, *ASME J. Heat Transfer*, vol. **123**, pp. 926–936, 2001.

Leach, R. N., Stevens, F., Langford, S. C., and Dickinson, J. T., Dropwise condensation: Experiments and simulations of nucleation and growth of water drops in a cooling system, *Langmuir*, vol. **22**, pp. 8864–8872, 2006.

Lee, Y. L., The wettability of solid surfaces modified by vacuum deposition of stearic acid, *Colloid Surf., A*, vol. **155**, nos. 2-3, pp. 221–229, 1999.

Leipertz, A., Dropwise condensation, in Stephan, sP., ed, VDI heat atlas VDI-GVC, 2nd ed., Springer, Germany, pp. 933–937, 2010.

Milinazzo, F. and Shinbrot, M., A numerical study of a drop on a vertical wall, *J. Colloid Interface Sci.*, vol. **121**, no. 1, pp. 254–264, 1988.

Poniewski, M. E. and Thome, J. R., *Nucleate Boiling on Micro-Structured Surfaces*, Heat Transfer Research, Inc., College Station, TX, USA, 2008.

Pozrikidis, C., *Fluid Dynamics: Theory, Computation, and Numerical Simulation*, 2nd ed., Springer, New York, 2009.

Rausch, M. H., Froba, A. P., and Leipertz, A., Dropwise condensation heat transfer on ion implanted aluminum surfaces, *Int. J. Heat Mass Transfer*, vol. **51**, pp. 1061–1070, 2008.

Rose, J. W., Condensation heat transfer fundamentals, *Chem. Eng. Res. Design*, vol. **76**, pp. 143–152, 1998.

Rose, J. W., Dropwise condensation theory and experiment: A review, *Proc. Inst. Mech. Eng.*, vol. **216**, pp. 115–128, 2002.

Santos, M. J. and White, J. A., Theory and simulation of angular hysteresis on planar surfaces, *Langmuir*, vol. **27**, no. 24, pp. 14868–14875, 2011.

Sikarwar, B. S., Battoo, N. K., Khandekar, S., and Muralidhar, K., Dropwise condensation underneath chemically textured surfaces: Simulation and experiments, *ASME J. Heat Transfer*, vol. **133**, no. 2, pp. 021501–021515, 2011.

Sikarwar, B. S., Khandekar, S., Agrawal, S., Kumar, S., and Muralidhar, K., Dropwise condensation studies on multiple scales, *Heat Transfer Eng., Special Issue: Adv. Heat Transfer*, vol. **33**, no. 3/4, pp. 301–341, 2012.

Sikarwar, B. S., Khandekar, S., and Muralidhar, K., Simulation of flow and heat transfer in a liquid drop sliding underneath a hydrophobic surface, *Int. J. Heat Mass Transfer*, vol. **57**, no. 2, pp. 786–811, 2013.

Tanasawa, I., Advances in condensation heat transfer, in *Advances in Heat Transfer*, Hartnett, J. P., Irvine, T. F., and Cho, I. Y., Eds., vol. **21**, pp. 57–59, Elsevier, New York, 1991.

Vemuri, S. and Kim, K. J., An experimental and theoretical study on the concept of dropwise condensation, *Int. J. Heat Mass Transfer*, vol. **49**, pp. 649–857, 2006.

Vemuri, S., Kim, K. J., Wood, B. D., Govindaraju, S., and Bell, T. W., Long term testing for dropwise condensation using self assembled monolayer coatings of n-octadecylmercaptan, *Appl. Therm. Eng.*, vol. **26**, no. 4, pp. 421–429, 2006.

Zhao, Q., Zhang, D. C., Lin, J. F., and Wang, G. M., Dropwise condensation on L–B film surface, *Chem. Eng. Process.*, vol. **35**, pp. 473–477, 1996.